RSC Advances

PAPER

View Article Online
View Journal | View Issue

Cite this: *RSC Adv.*, 2019, **9**, 42163

Solvothermal synthesis and modification of $NaYF_4$:Yb/Er@$NaLuF_4$:Yb for enhanced up-conversion luminescence for bioimaging†

Hua Li, Xuguang Liu and Xia Li *

Received 30th October 2019
Accepted 12th December 2019

DOI: 10.1039/c9ra08921g

rsc.li/rsc-advances

Water-soluble $NaYF_4$:Yb/Er@$NaLuF_4$:Yb up-converting nanoparticles (UCNPs) with a strong green emission were successfully prepared by a solvothermal method in a short period of time and at a low temperature. First, the hydrophobic UCNPs were prepared by a simple solvothermal method, then modified using a polyetherimide (PEI) surfactant or oxidation of the oleic acid ligands with the Lemieux-von Rudloff reagent. The modified UCNPs, having an average particle diameter of 60 ± 5 nm, showed a high dispersity. The oleic acid ligand on the sample surface was oxidized azelaic acid ($HOOC(CH_2)_7COOH$), identified from Fourier transform infrared (FTIR) spectroscopy, which results in the generation of free carboxylic acid, hence conferring a high solubility in water. The 3-4,5-dimethylthiazol-2-yl-2,5-diphenyl tetrazolium bromide (MTT) method and cell-targeted labeling proved that oleic acid-capped UCNPs after oxidation (UCNPs-OAO) have a higher biocompatibility than polyetherimide-capped UCNPs (UCNPs-PEI). Therefore, the UCNPs-OAO have a great potential in biomedical applications, such as multimodal imaging, targeted therapy, and gene therapy.

Introduction

Rare-Earth (RE) doped up-converting luminescent materials exhibit unique properties of high-energy emission under near-infrared excitation, which makes them attractive for bioimaging. Compared with semiconductor quantum dots and organic dyes, rare-earth doped up-converting luminescent materials are non-toxic, have good optical stability, and low background fluorescence interference. In addition, light scattering that occurs when the light source penetrates the biological tissue can be significantly reduced under near-infrared excitation,[1–17] making it suitable for cancer diagnosis, drug delivery, and gene therapy.[18–22]

Among the many up-converting luminescent hosts, fluoride systems have lower phonon energy, more metastable energy series, and a higher up-conversion luminescence efficiency.[23] Therefore, sodium tetrafluoroidal ($NaYF_4$) and sodium tetrafluoroquine ($NaLuF_4$) crystals has been considered as the best up-converting luminescent host materials in recent years. Although great progress has been made in the synthesis of up-converting luminescent materials based on $NaYF_4$, especially those with controllable morphology and size, the luminescence efficiency of the materials is still not very high due to the high surface defects, the easy interaction between rare earth ions, and the low quantum yield.[24] Therefore, it is necessary to use a core–shell structure because it can not only suppress concentration quenching, but can also separate different rare-earth doped ions in the core–shell space. This way, the up-conversion luminescence efficiency could be further improved.[25–30] For example, Chow *et al.*[31] prepared $NaYF_4$:Yb, Er@$NaYF_4$:Yb,Tm nanocrystals, and demonstrated that the core–shell structure increased the quantum efficiency by anywhere from 7 to 29 times. Li Fuyou *et al.*[32] demonstrated that a core–shell structure reduced cross-relaxation and surface quenching effects by introducing a CaF_2 layer to improve the up-conversion emission. Although a core–shell structure can effectively improve the luminescence efficiency of up-converting luminescent materials, it cannot change the surface function group of the up-converting nanoparticles (UCNPs) with oleic acid ligands prepared by conventional methods, which limits its application in biology. Therefore, the primary requirement for up-converting luminescent bioprobes is the presence of hydrophilic groups on the sample surface and good biocompatibility. The main avenue for the preparation of biocompatible UCNPs is surface functionalization using a SiO_2 coating,[33] an amphiphilic polymer coating,[34] and ligand exchange.[35] Although these methods can effectively improve the hydrophilicity, the process is complex. Therefore a simple way to modify the surface of these up-converting nanoparticles is a priority.

To date, a few studies have reported on anisotropic β-$NaYF_4$:Yb,Er NCs prepared through a solvothermal method. For example, the Huang group researched the synthesis of tridoped $NaYF_4$:Sc^{3+}/Er^{3+}/Yb^{3+} nanoparticles by a solvothermal method

College of Materials Science and Engineering, Qingdao University of Science & Technology, Qingdao 266042, PR China. E-mail: Lix@qust.edu.cn

† Electronic supplementary information (ESI) available. See DOI: 10.1039/c9ra08921g

that took 48 h.[36] The Wuang group reported the synthesis of $Na(Y_{1.5}Na_{0.5})F_6$ single-crystal nanorods *via* a solvothermal method at lasting 24 h.[37] Therefore, it is a challenge to prepare UCNPs with good performance by a solvothermal method in a short time. In 2015, our group found that the addition of Na_2HPO_4 reduces the reaction temperature (down to 200 °C) during cubic-to-hexagonal crystal transition.[38] In this study, we reported the synthesis of hydrophilic $NaYF_4$:Yb/Er@$NaLuF_4$:Yb UCNPs with a strong green emission using a solvothermal method that only lasted 4 h at 180 °C. Then the UCNPs were modified by a PEI surfactant or through the oxidation of the oleic acid ligands with the Lemieux-von Rudloff reagent. This system is not known to have been reported in literature to this date. Finally, we compared the luminescence properties and the application of UCNPs-OAO and UCNPs-PEI for bioimaging.

Experimental

Chemicals

Erbium oxide (Er_2O_3), lutecium oxide (Lu_2O_3), ytterbium oxide (Yb_2O_3), and yttrium oxide (Y_2O_3) were purchased from Shanghai Yuelong Non-Ferrous Metals company (Shanghai, China). Polyetherimide (PEI) (analytical reagent (AR), 99%) was purchased from Xiya Chemical Reagent company (Shandong, China). NaF (AR, 98%) and K_2CO_3 (AR) were purchased from Sinopharm Chemical Reagent company (Shandong, China). Stearic acid (AR) was purchased from Xiya Chemical Reagent company (Chengdu, China). *t*-Butanol (AR), cyclohexane (AR), NaOH (AR, 96%), hydrochloric acid (AR), oleic acid (AR), and nitric acid (AR) were purchased from Tieta Chemical company (Yantai, China). Phosphate buffer salt solution (PBS) (0.01 M) and Tris–HCl buffer salt solution (TBS) (pH = 7.2–7.5) were purchased from Solarbio company (Beijing, China). Bovine serum albumin was purchased from Oberson company (Beijing, China). Qingdao University provided the human cervical cancer cells (HeLa cells). The cell culture medium (RPMI 1640) was purchased from GIBCO, United States.

Synthesis of the $NaYF_4$:Yb/Er@$NaLuF_4$:Yb nanoparticles

First, $NaYF_4$:Yb/Er particles were synthesized. 5 mM NaF, 15 mL H_2O, 15 mL ethanol, and 1 mM rare earth stearates (Y : Yb : Er = 78% : 20% : 2%) that were synthesized according to a previous report[39] were added to a beaker. Then, the above solution was poured into a 50 mL Teflon bottle and heated to 120 °C for 2 h. The products were obtained after washing with ethanol and water several times, and then drying at 80 °C for 12 h.

The synthesized $NaYF_4$:Yb/Er nanoparticles were used as seeds for shell heteroepitaxial growth. 1 mM $RE(NO_3)$ (Lu : Yb = 7 : 3) and 5 mL oleic acid (OA) were added to a mixture of ethylene glycol (EG, 15 mL) and water (10 mL). The pH was adjusted to 8.5 using 2 M NaOH and HNO_3. After stirring for 10 min, $NaYF_4$:Yb/Er (0.5 g) and 1 mL HF were added to the beaker. Then, the mixture was stirred, and the pH was adjusted to 2.5 using 2 M NaOH and HNO_3. The mixture was transferred to a 50 mL Teflon bottle and then heated to 180 °C for 4 h. The final products were obtained after washing them with a 1 : 6 trichloromethane/ethanol solution followed by a 1 : 2 water/ethanol solution several times, and then dried at 80 °C overnight.

Surface-modified nanoparticles

The synthesis of oleic acid-capped UCNPs after oxidation (UCNPs-OAO) was performed as follows: 0.10 g of prepared UCNPs were weighed accurately and were added to a beaker containing a mixture of 10 mL distilled water, 70 mL *t*-butanol, 5 mL K_2CO_3 (5 wt%) and 100 mL cyclohexane and was well mixed. Then, a certain amount of Lemieux-von Rudloff reagent (solution of 0.105 mM $NaIO_4$ and 5.7 mM $KMnO_4$) was added to the beaker containing the above mixture and was heated to 40 °C, stirred for 3 h, and then centrifuged. After centrifugation, the sample was transferred to a 50 mL hydrochloric acid solution (pH = 4–5) and stirred. Then, it was washed twice with deionized water and dried at 80 °C overnight. The synthesis of polyetherimide-capped UCNPs (UCNPs-PEI) was performed as follows: the UCNPs-PEI were obtained by the previous method while replacing the oleic acid with polyetherimide. 0.02 g of the prepared UCNPs in 2 mL hexane and 0.02 g polyetherimide in 2 mL ethanol were mixed, ultrasonicated for 30 min, and stirred for 6 h. Finally, the powder was obtained through centrifugation and drying.

Cell culture and cytotoxicity assay of the surface-modified nanoparticles

HeLa cells were maintained in RPMI 1640 medium supplemented with 10% fetal bovine serum, and were incubated in 5% CO_2 humidified at 37 °C according to published protocols.[35,40] The number of viable HeLa cells after treatment with modified-sample was evaluated by the MTT assay. Cellular uptake by HeLa cancer cells was recorded on an inverted fluorescence microscope. Then, 200 μg mL^{-1} of up-converting TBS buffer was dispersed into 2 mL of the cell culture medium, and incubated at 37 °C for 2 h. Finally, the samples needed for the test were prepared according to a published protocol.[41]

Characterization

X-ray diffraction (XRD), using Cu Kα = 1.5406 Å, was used to probe the crystal structure of the samples. Transmission electron microscopy (TEM) and high-resolution TEM (HR-TEM), using a JEOL JEM-2010 instrument at an accelerating voltage of 200 kV, was used to characterize the morphology of samples. The Fourier transform infrared (FT-IR) spectra were measured using a Brüker TENSOR-27 spectrometer with the samples in KBr pellets. The Hitachi F-4600 spectrophotometer (Tokyo, Japan) and Edinburgh fls1000 recorded up-conversion spectra of samples and excitation state life of rare earth ion using a 980 nm laser diode, respectively. Digital camera (Nikon D300) recorded the solubility and luminescence properties of samples in aqueous solution. Confocal imaging of the cells was performed using a modified Olympus FV1000 laser-scanning confocal microscope (LSCM) equipped with a continuous-

wave (CW) near-infrared (NIR) laser at 980 nm (Connet Fiber Optics, China).

Results and discussion

XRD analysis

Fig. 1 shows the crystal structure of α-$NaYF_4$:Yb/Er (a) and α-$NaYF_4$:Yb/Er@β-$NaLuF_4$:Yb (b–d) prepared by a solvothermal method that took 4 h at 180 °C. As can be seen from Fig. 1a, the diffraction peak positions of the sample matched the data for the cubic phase (PDF file no. 77-2042). All of the crystal structures of the α-$NaYF_4$:Yb/Er@β-$NaLuF_4$:Yb nanoparticles appear to be a cubic and hexagonal mixed structure after heteroepitaxial growth in Fig. 1(b and c). The diffraction peaks of the synthesized core–shell nanoparticles can be indexed as mixed phases, which match the standard cards of β-$NaLuF_4$ (PDF file no. 27-726) and α-$NaYF_4$ (PDF file no. 77-2042). This is a preliminary indication of the presence of a β-$NaLuF_4$ crystal in the sample. However, only the diffraction peak of the hexagonal $NaLuF_4$:Yb was observed in Fig. 1d when the reaction time is 4 h and matches the standard card (PDF file no. 27-726). In addition, we also can see from the magnification of 2θ from 29.4° to 31.1° in the upper right corner, that the intensity of the β-$NaLuF_4$ diffraction peak of the core–shell particles becomes gradually more intense with a longer reaction time. This is because the heterogeneous interface between the core and the shell leads to the growth of the hexagonal phase of the shell, which is consistent with previous observations by Chen and co-workers.[42] Importantly, an increase in the intensity of the β-$NaLuF_4$ diffraction peak means an increase in the content of β-$NaLuF_4$, resulting in an increase in the luminescence intensity of the sample. Zhao and Li *et al.* reported that they obtained pure hexagonal phase $NaYF_4$:Yb/Er by a solvothermal method at 200–300 °C.[43,44] Chen and co-workers[42] prepared α-$NaGdF_4$ core nanocrystals by a solvothermal method at 180 °C. The preparation temperature of their experiments is higher than ours (120 °C), highlighting an obvious advantage to this work.

In the previous report,[45–48] the stable alpha-phase is often the first formed when prepared by wet chemical methods due to a small size-effect. This is a common phenomenon that the smaller nanoparticles tend to have a more symmetrical crystal structure in nanosystems, so alpha-phase (high symmetry) is easier to form than hexagonal phase (low symmetry). Nevertheless, the number of effective collisions and exchanges between Lu^{3+} and Y^{3+} will increase as the reaction time increases, which can lead to the growth and transformation of crystals. The results in Fig. 1 fit well with this rule.

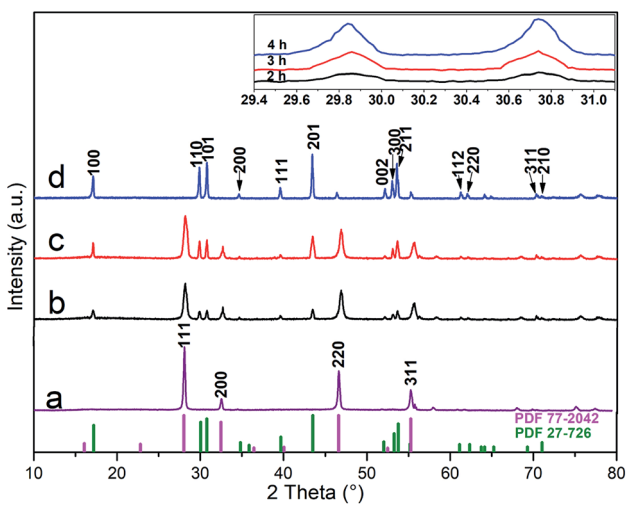

Fig. 1 XRD patterns of $NaYF_4$:Yb/Er (a) and $NaYF_4$:Yb/Er@$NaLuF_4$:Yb with reaction time of 2 h (b), 3 h (c), 4 h (d), respectively. The inset shows a magnified patterns of 2θ about 30°C and the bottom part is the lines pattern of the hexagonal phase (PDF 27-726) $NaLuF_4$ and cubic phase (PDF 77-2042) $NaYF_4$, respectively.

Morphology analysis

As can be seen from the Fig. 2a, α-$NaYF_4$:Yb, Er nanoparticles with an average particle size of about 35 nm are spherical, uniform in morphology, and have a narrow in size distribution. These particles also show lattice spacing of approximately 0.318, according to the HR-TEM scan, which is accorded with the XRD data (JCPDS card no. 77-2042). This indicates that the nanoparticles are enclosed by {111} facets. In order to study the growth process of core–shell nanoparticles, we prepared core–shell nanoparticles at each reaction time and stage of the heteroepitaxial growth. Fig. 2(b–d) shows the SEM images of α-$NaYF_4$:Yb,Er/β-$NaLuF_4$:Yb nanoparticles at different reaction times. As shown in the figure, the morphology of the sample remains essentially the same during the entire growth process from core to core–shell, and all of the particles were spherical. However, the size of the nanoparticles increases gradually with the increase in reaction time. The particle size of α-$NaYF_4$ crystal nucleus is 35 nm, and the diameter of heterogeneous core–shell nanoparticles increases to 50 nm, 55 nm and 60 nm when the heteroepitaxial growth time is 2, 3 and 4 h. We can clearly see lattice boundaries from HR-TEM images, and the lattice spacing is about 0.295 nm, which matches the (110) crystal plane spacing of β-$NaLuF_4$. Therefore, we can further show that α-$NaYF_4$:Yb,Er/β-$NaLuF_4$:Yb nanoparticles have been successfully prepared by increasing the size of core–shell nanoparticles, through analyzing the appearance of β-$NaLuF_4$ lattice stripes in HR-TEM, and by combining the data with the X-ray diffraction data of core and core–shell nanoparticles in Fig. 1.

Fig. 2(e and f) shows morphologies of modified-nanoparticles (UCNPs-OAO and UCNPs-PEI) with about a 60 nm diameter. The morphology and size of modified-nanoparticles did not change compared with $NaYF_4$:Yb/Er@$NaLuF_4$:Yb. As can be seen from the elemental mapping images (Fig. 2g), a single particle, contains a distribution area where Y content is smaller than that of Lu and Yb, which indicates that Y exists in an internal nuclear crystal, while Lu and Yb are distributed in the outer shell. This result strongly proves the formation of α-$NaYF_4$:Yb,Er/β-$NaLuF_4$:Yb core–shell nanoparticles. The energy dispersive spectroscopy (EDS) (Fig. 2f) demonstrated that Lu, Y, Yb, and Er were present in the as-prepared sample, and the peak intensity of Y is lower than

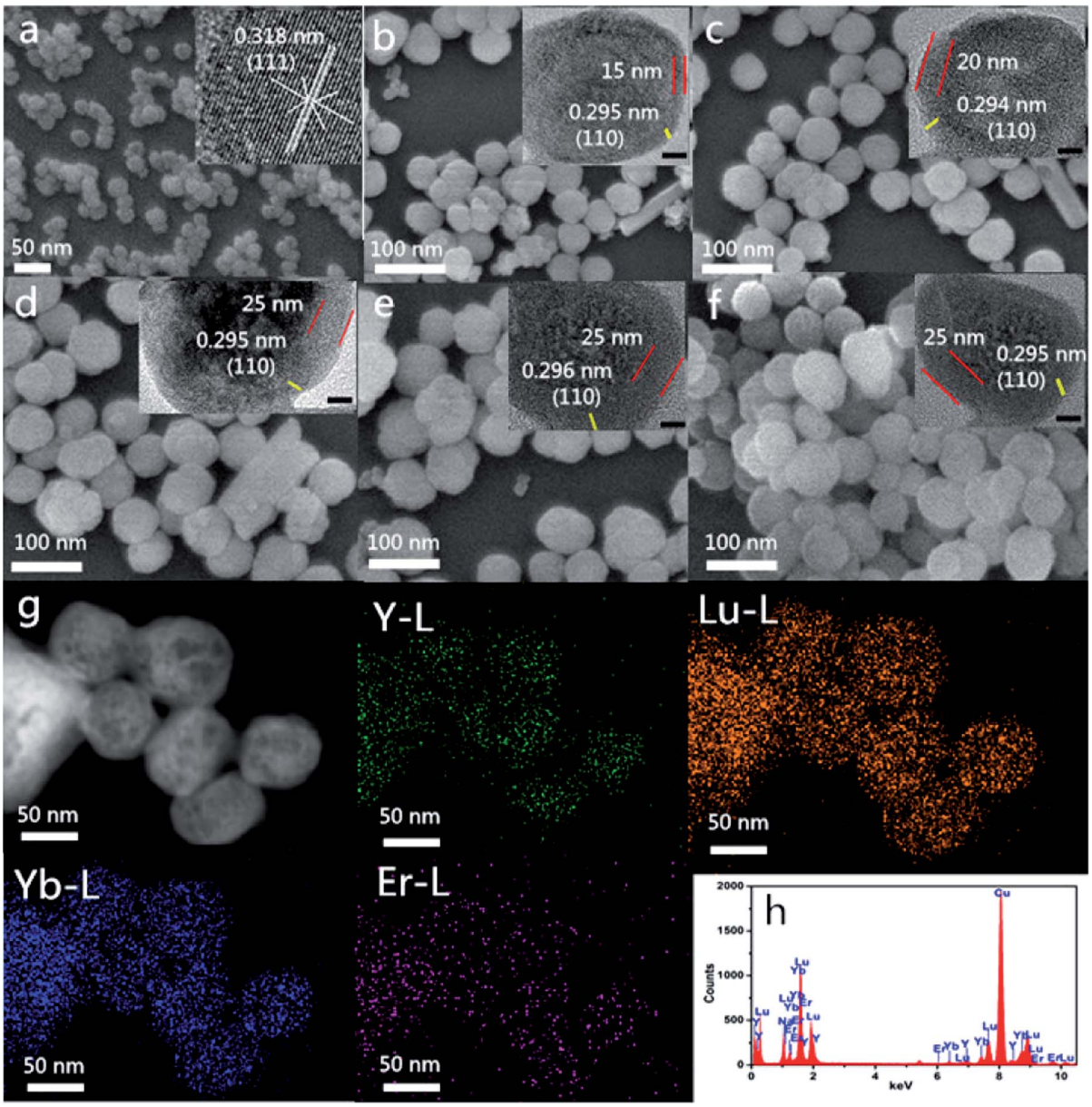

Fig. 2 SEM images of $NaYF_4$:Yb/Er (a), $NaYF_4$:Yb/Er@$NaLuF_4$:Yb with reaction time of 2 h (b), 3 h (c), 4 h (d), UCNPs-OAO (e), UCNPs-PEI (f), respectively; elemental mapping and EDS of $NaYF_4$:Yb/Er@$NaLuF_4$:Yb with reaction time of 4 h (g) and (h), respectively. Insets in (a)–(f) show HR-TEM images of UCNPs. Scale bars represent 20 nm for insets.

that of Lu when the molar number is the same. This result once again shows that Y exists in the inner core, while Lu exists in the shell.

Luminescence study

Fig. 3a shows fluorescence spectra and luminescence photographs of $NaYF_4$:Yb/Er and $NaYF_4$:Yb/Er@$NaLuF_4$:Yb nanoparticles excited by 980 nm diode laser. Fig. 3, illustrates that at 980 nm excitation, there are three distinct characteristic peaks at 523 nm, 541 nm, and 657 nm. At 541 nm, the intensity of $NaYF_4$:Yb/Er@$NaLuF_4$:Yb is about 40–50 times that of $NaYF_4$:-Yb/Er, which is corroborated by the XRD results. The shell modified by Yb^{3+} is quite important in sustaining the excitation energy and achieves an effective energy transfer toward nanocore surfactants, resulting in the luminous intensity being improved significantly. Fig. 3a also indicates that the luminescence intensity of $NaYF_4$:Yb/Er@$NaLuF_4$:Yb nanoparticles with reaction time of 4 h is much higher than that of 2 h and 3 h. The reason is that the growth process of the shell is not complete at the shorter times and the proportion of β-$NaLuF_4$ on the shell is small when the reaction time is 2 h, so the luminescence intensity is lower. The hexagonal phase on the shell increases and the luminescence intensity increases at 4 h, which is consistent with the results of XRD analysis. In summary, the core–shell $NaYF_4$:Yb/Er@$NaLuF_4$:Yb nanoparticles with the highest luminescence intensity were prepared at reaction time

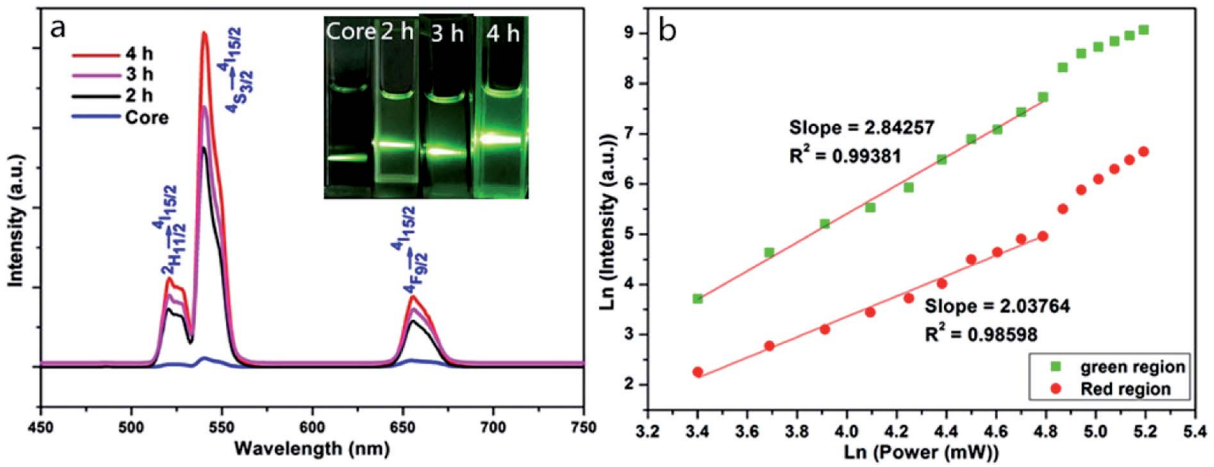

Fig. 3 Upconversion emission spectra of $NaYF_4$:Yb/Er and $NaYF_4$:Yb/Er@$NaLuF_4$:Yb (0.3 g powder) with different reaction time excited by 980 nm CW diode laser (a); insets in (a) show luminescence photographs of UCNPs dispersed in cyclohexane. Red and green emission intensity relationship with dependence of the laser pump power for the $NaYF_4$:Yb/Er@$NaLuF_4$:Yb with reaction time of 4 h (b).

of 4 h. The dependence of the red-green emission intensity on the laser pump power for the $NaYF_4$:Yb/Er@$NaLuF_4$:Yb with a reaction time of 4 h is shown in Fig. 3b. It indicates that green and red emissions are three-photon and two-photon transfer processes, respectively.

FTIR analysis

Fig. 4 shows the infrared spectra of the modified $NaYF_4$:Yb/Er@$NaLuF_4$:Yb. All spectra reveal a wide band centered at 3410 cm^{-1} related to the O–H stretching vibrations. These vibrations are mainly from the surface of the nanoparticles with assimilated H_2O molecules. Symmetric and antisymmetric vibrational peaks at 2913 cm^{-1} and 2825 cm^{-1} of methylene were as attributed to the oleic acid. The absorption peaks in the 1590–1420 cm^{-1} range can be attributed to the stretching vibration absorption peaks of the carboxyl group, and are also observed in the samples (Fig. 4a and b), confirming the presence of oleic acid in the nanomaterials synthesized. It is also evident from Fig. 4a and b that the absorption peaks at 1533 cm^{-1} and 1420 cm^{-1} in the samples after oxidation are intensified, indicating that UCNPs-OAO have a larger number of carboxyl groups. Fig. 4c shows the five characteristic absorption bands for PEI: 3444 cm^{-1} for N–H stretching, 2934 cm^{-1} and 2856 cm^{-1} for C–H stretching vibrations, 1630 cm^{-1} and 1573 cm^{-1} for N–H stretching, and confirmed the capping of PEI on the surface of the UCNPs. UCNPs-OAO also showed a stronger stretching vibration absorption peak for the carboxyl groups in the 1590–1420 cm^{-1} range as compared with UCNPs-PEI. Since the carboxyl group is hydrophilic, this makes the UCNPs-OAO more promising for biological application.

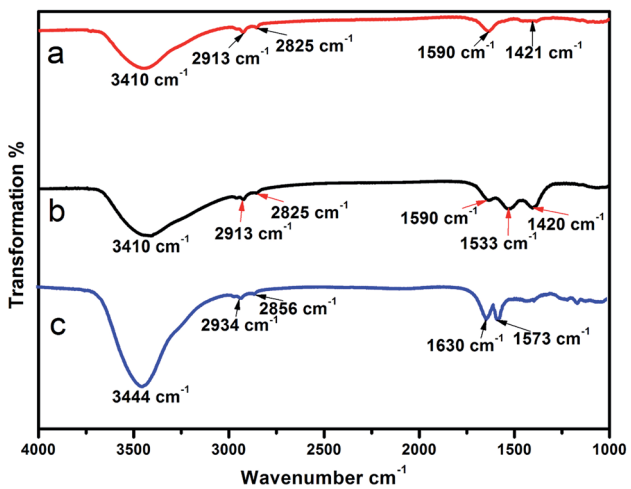

Fig. 4 FTIR spectra of the surface modified samples: $NaYF_4$:Yb/Er@$NaLuF_4$:Yb (a), UCNPs-OAO (b) and UCNPs-PEI (c).

Luminescence study of surface-modified samples

Fig. 5a shows fluorescence spectra and luminescent photographs of different samples of nanoparticles excited at 980 nm. The figure shows that the three materials exhibit fluorescence emission peaks at 525 nm, 542 nm, and 660 nm, which are matched to the energy level transitions of the Er^{3+} ion, for $^2H_{11/2}$ to $^4I_{15/2}$, $^4S_{3/2}$ to $^4I1_{5/2}$, and $^4F_{9/2}$ to $^4I_{15/2}$, respectively. The first two are green emissions whereas the last one is a red emission.[49] The spectra show that the intensity of the UCNPs-OAO is about 2–3 times that of the UCNPs-PEI. And the energy level lifetime of the $^4S_{3/2}$ (923.8 μs) and $^4F_{9/2}$ (1381.3 μs) of Er^{3+} of UCNPs-OAO is higher than that of UCNPs-PEI (see Fig. S2 and Table S1 of the ESI for details†). From the luminescent photographs, we can see that all three samples emit green light, and the color intensities of $NaYF_4$:Yb/Er@$NaLuF_4$:Yb and UCNPs-OAO are similar, but the color intensity of UCNPs-PEI is weaker than that of the other two, which is in accordance with the results of fluorescence spectra. Therefore, UCNPs-OAO is more suitable for bioimaging experiments. As shown in Fig. 5b, the core–shell nanoparticle absorb near-infrared light *via* Yb^{3+} (red shell) and subsequently transfer the energy to Yb^{3+}, Er^{3+} (green core), which leads to up-converted green and red emissions.

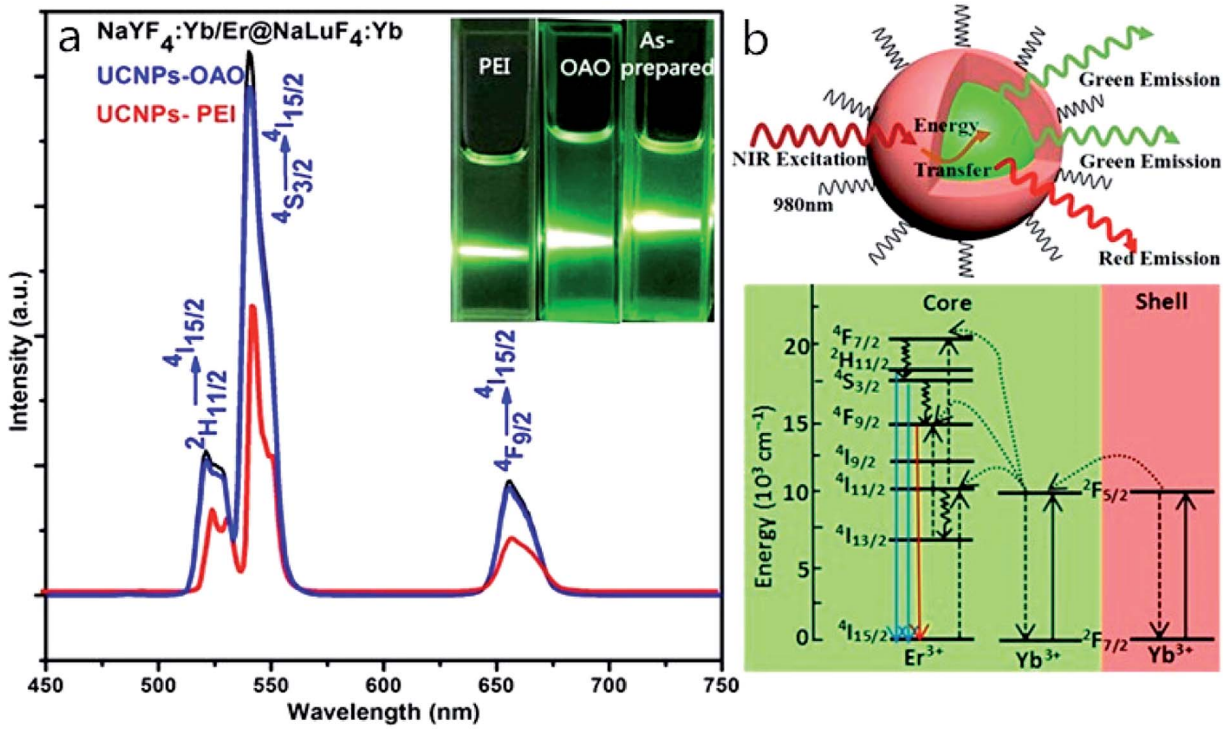

Fig. 5 Upconversion emission spectra of $NaYF_4$:Yb/Er@$NaLuF_4$:Yb, UCNPs-PEI and UCNPs-OAO (0.3 g powder) excited by 980 nm CW diode laser (a). Insets in (a) show luminescence photographs of UCNPs dispersed in cyclohexane or water. Schematic illustration and energy level diagram (bottom) of core–shell nanoparticles excited by 980 nm laser (b).

Cytotoxicity study

In order to efficiently label the cells, it is necessary to consider whether intracellular UCNPs are cytotoxic.[50–54] The cell survival rates with UCNPs-OAO and UCNPs-PEI at different doses were first examined by the MTT assay. Fig. 6 summarizes the results of the cytotoxicity study. The cell viability of the control group was set to 100%. Statistical results showed that the survival rates in the presence of both UCNPs-OAO and UCNPs-PEI were

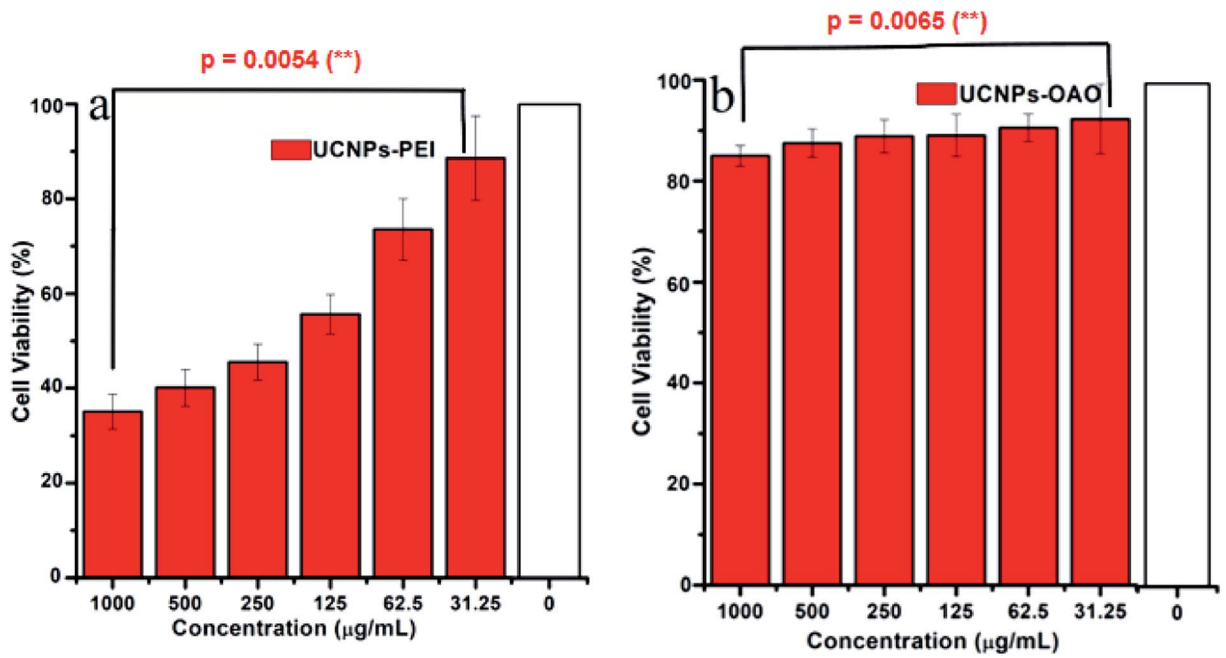

Fig. 6 Viability of HeLa cell incubated with different concentrations of surface-modified up-conversion nanoparticles at 37 °C. (a) UCNPs-PEI, (b) UCNPs-OAO.

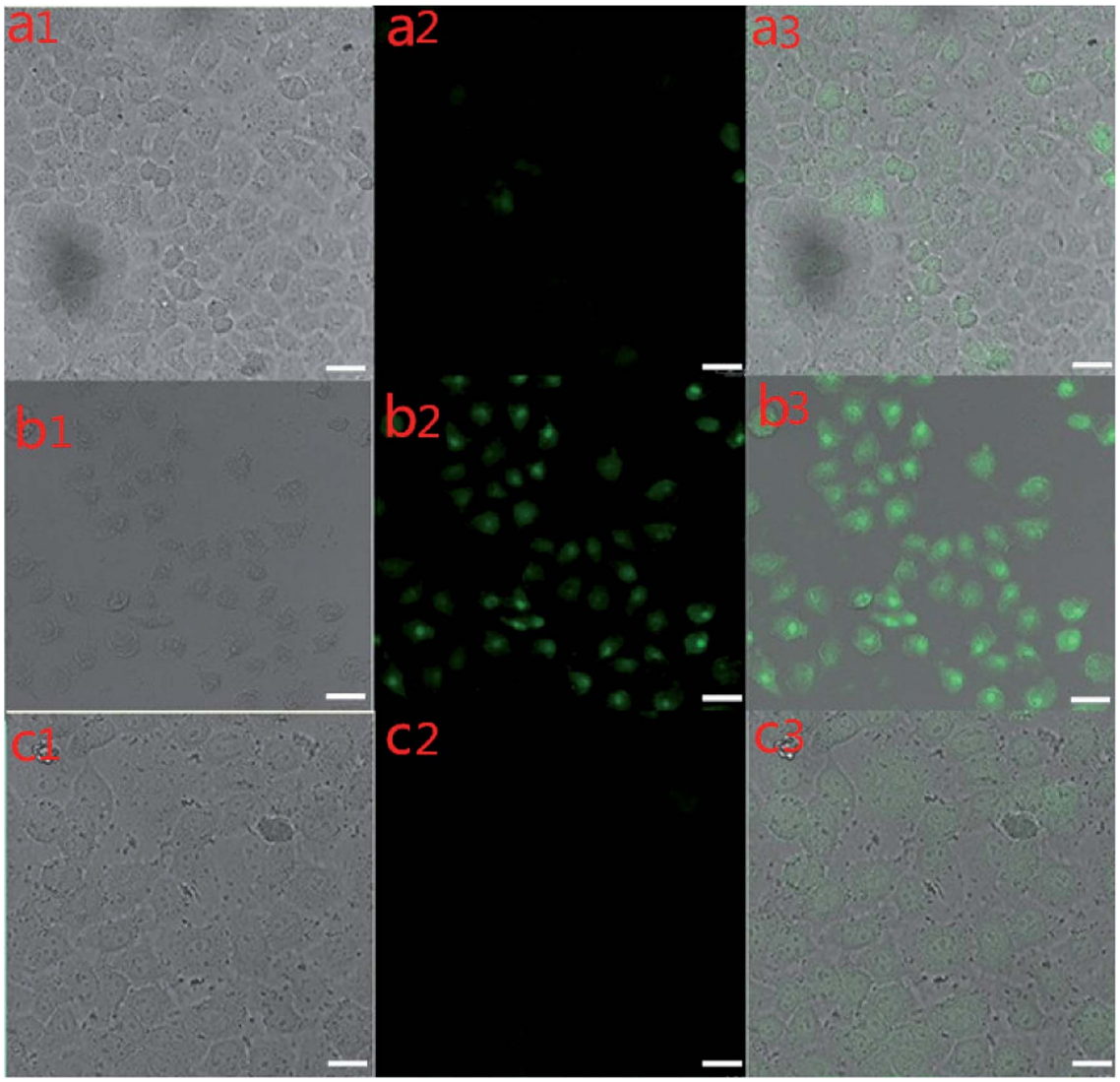

Fig. 7 Confocal fluorescent images of HeLa cells collected at bright field (left), black field (middle) and merged (right), respectively. HeLa cells incubated with UCNPs-OAO for 1 h (a), 2 h (b) at 37 °C; (c) HeLa cells incubated with UCNPs-PEI for 2 h at 37 °C; UCL signals were collected at 510–560 nm, $\lambda_{ex} = 980$ nm. Scale 20 μm.

significantly lower than those of the control. And there is an extremely significant discrepancy between the 31.5 μg mL^{-1} UCNPs and the 1000 μg mL^{-1} UCNPs ($P_{UCNPs\text{-}PEI} = 0.0054$, $P_{UCNPs\text{-}OAO} = 0.0065$). The cell survival rate reached 90% at low doses of UCNPs (31.5 μg mL^{-1}). At high doses of UCNPs (1000 μg mL^{-1}), the cell survival rate with UCNPs-OAO reached 85% whereas that for UCNPs-PEI only reached 35%. As shown, the cytotoxicity of UCNPs-OAO was lower than that of UCNPs-PEI when the dose of UCNPs was 200 μg mL^{-1}. Therefore, UCNPs-OAO can be used as probes for tumor cell imaging.

Cellular uptake study

The targeted imaging of cancer cells was performed on an inverted fluorescence microscope. First, the HeLa cells were hatched with UCNPs-OAO for 1 h at 37 °C. However, Fig. 7(a1–a3) shows a weak up-conversion luminescence (UCL) signal in the HeLa cells. The HeLa cells appeared to have strong luminescence as the culture time was extended to 2 h, as shown in Fig. 7(b1–b3). The results indicated that UCNPs could not enter the HeLa cells without enough incubation time. When the HeLa cells were hatched with UCNPs-PEI for 2 h at 37 °C, a signal was also detected at an excitation of 980 nm (Fig. 7(c1–c3)), but this signal was weaker than that of UCNPs-OAO nanoparticles cultured with HeLa cells under the same conditions. By comparing the intensity of the cells incubated with UCNPs-PEI and UCNPs-OAO, we concluded that the latter is more suitable for bio-targeting. In addition, the targeting images and bright field images of the cells overlapped greatly. UCNPs-OAO has achieved targeted tumor cell imaging, indicating that it has a prospective application in early detection of tumors. UCNPs-OAO is a better cell marker as compared to UCNPs-PEI, which also corroborates the results from the MTT test.

Conclusion

$NaYF_4$:Yb/Er@$NaLuF_4$:Yb core–shell nanoparticles with a strong green light emission were successfully prepared by a solvothermal method with a 4 h reaction time. Then, the nanoparticles were either modified with oleic acid ligands on the surface (UCNP-OAO) to form nanoparticles with carboxyl groups or were modified with polyetherimide (UCNPs-PEI) to create nanoparticles with amino groups on the surface. The XRD indicates that crystal structures of the α-$NaYF_4$:Yb/Er@β-$NaLuF_4$:Yb nanoparticles appear to be a pure hexagonal structure when the reaction time is 4 h. The TEM and HR-TEM images demonstrates that all of the particles were spherical and the morphology of modified-nanoparticles did not change compared with $NaYF_4$:Yb/Er@$NaLuF_4$:Yb core–shell nanoparticles. The fluorescence spectra shows that the UCNPs-OAO exhibit strong green fluorescence emission peaks at 542 nm, which are matched to the energy level transitions of the Er^{3+} ion, for $^4S_{3/2}$ to $^4I_{15/2}$. The cytotoxicity of the functionalized UCNPs-OAO and UCNPs-PEI nanoparticles was evaluated using the MTT assay, with the results indicating that the cytotoxicity of UCNPs-OAO was lower than that of UCNPs-PEI. This data provided the experimental basis for the targeted imaging of HeLa cells. Therefore, UCNPs-OAO can offer a effective tool for medical application, such as gene therapy, drug delivery, and cancer diagnosis.

Conflicts of interest

There are no conflicts of interest to declare.

Acknowledgements

This research was supported by the National Natural Science Foundation of China (Grants: 51372127).

References

1 T. Pang and W. Lu, *Ceram. Int.*, 2017, **43**, 1061–1065.
2 M. Zhao, Z. G. Xia, M. S. Molokeev, L. X. Ning and Q. L. Liu, *Chem. Mater.*, 2017, **29**, 6552–6559.
3 J. Jiu, X. An, J. Li, *et al.*, *Dalton Trans.*, 2017, **46**, 15954–15960.
4 L. Shi, J. Hu, X. Wu, *et al.*, *Dalton Trans.*, 2018, **47**, 16445–16452.
5 Y. H. Xiao, Z. P. Deng, Z. B. Zhu, *et al.*, *Dalton Trans.*, 2017, **46**, 16493–16504.
6 J. H. Chung, J. H. Ryu, S. Y. Lee, S. H. Kang and K. B. Shim, *Ceram. Int.*, 2013, **39**, 1951–1956.
7 L. L. Zhu, Y. J. Park, L. Gan, S. I. Go, H. N. Kim, J. M. Kim and J. W. Ko, *Ceram. Int.*, 2017, **43**, 8525–8530.
8 F. Wang, D. Banerjee, Y. Liu, X. Chen and X. Liu, *Analyst*, 2010, **135**, 1839–1854.
9 F. Wang and X. Liu, *Chem. Soc. Rev.*, 2009, **38**, 976–989.
10 S. Wang, K. Liu and J. Liu, *Angew. Chem. Int. Ed.*, 2011, **50**, 3084–3088.
11 X. M. Li, F. Zhang and D. Zhao, *Nano Today*, 2013, **8**, 643–676.
12 F. C. Veggel, C. Dong, N. J. Johnson and J. Pichaandi, *Nanoscale*, 2012, **4**, 7309–7321.
13 Y. Zhang, L. Zhang, R. Deng, J. Tian, Y. Zong, D. Jin and X. Liu, *J. Am. Chem. Soc.*, 2014, **136**, 4893–4896.
14 L. Wang, X. Li and Z. Li, *Adv. Mater.*, 2015, **27**, 5528–5533.
15 A. M. El-Toni, M. A. Habila and J. P. Labis, *Nanoscale*, 2016, **8**, 2510–2540.
16 H. Chen, F. Lang and Y. Zhang, *J. Mater. Chem. C*, 2015, **3**, 6314–6321.
17 G. Chen, T. Y. Ohulchanskyy and A. Kachynski, *ACS Nano*, 2011, **5**, 4981–4987.
18 J. Wang, F. Wang and C. Wang, *Angew. Chem., Int. Ed.*, 2011, **50**, 10369–10372.
19 E. M. Chan, E. S. Levy and B. E. Cohen, *Adv. Mater.*, 2015, **27**, 5753–5761.
20 X. Xie, Z. Li and Y. Zhang, *Small*, 2017, **13**, 1–15.
21 M. H. Chan, Y. T. Pan and I. J. Lee, *Small*, 2017, **13**, 1–12.
22 D. Yang, Y. Dai and P. Ma, *Chem.–Eur. J.*, 2013, **19**, 2685–2694.
23 L. Wang, X. Li and Z. Li, *Adv. Mater.*, 2015, **27**, 5528–5533.
24 H. Lu, G. Yi and S. Zhao, *J. Mater. Chem.*, 2004, **14**, 1336–1341.
25 Q. Su, S. Han and X. Xie, *J. Am. Chem. Soc.*, 2012, **134**, 20849–20857.
26 Y. Dai, H. Xiao and J. Liu, *J. Am. Chem. Soc.*, 2013, **135**, 18920–18929.
27 Y. Zhong, G. Tian and Z. Gu, *Adv. Mater.*, 2014, **26**, 2831–2837.
28 G. S. Yi and G. M. Chow, *Chem. Mater.*, 2007, **19**, 341–353.
29 B. B. Ding, H. Y. Peng and H. S. Qian, *Adv. Mater. Interfaces*, 2016, **3**, 1500649.
30 M. L. Zhao, L. N. Hao, J. Zhang, C. Y. Zhang, Y. Lu and H. S. Qian, *Langmuir*, 2019, **35**, 489–494.
31 D. Yang, C. Li, G. Li, M. Shang, X. Kang and J. Lin, *J. Mater. Chem.*, 2011, **21**, 5923–5927.
32 Y. Li, Y. Gu, W. Yuan, T. Cao, S. P. Yng, Z. G. Zhou and F. Y. Li, *ACS Appl. Mater. Interfaces*, 2016, **8**, 19208–19223.
33 X. D. Zhang, X. Jin and D. F. Wang, *Phys. Status Solidi C*, 2011, **7**, 1128–1131.
34 T. Passuello, M. Pedroni and F. Piccinelli, *Nanoscale*, 2012, **4**, 7682–7689.
35 W. Kong, T. Sun and B. Chen, *Inorg. Chem.*, 2017, **56**, 872–877.
36 Q. Huang, J. Yu and E. Ma, *J. Phys. Chem. C*, 2010, **114**, 4719–4724.
37 L. Wang and Y. Li, *Nano Lett.*, 2006, **6**, 1645–1649.
38 M. Lv and X. Li, *Mater. Des.*, 2015, **88**, 514–519.
39 R. S. Zhou and X. Li, *Opt. Mater. Express*, 2016, **6**, 1313–1320.
40 S. H. Medina, G. Tiruchinapally and M. V. Chevliakov, *Adv. Healthc. Mater.*, 2013, **2**, 1337–1350.
41 R. Lv and P. Yang, *ACS Nano*, 2015, **9**, 1630–1647.
42 H. Chen, P. Zhang and H. Cui, *Nanoscale Res. Lett.*, 2017, **12**, 548–556.
43 Y. Hu, B. Wu, Q. Ji, X. Y. Wang, Y. Li, Y. X. Sun, J. Z. Huo and X. J. Zhao, *Talanta*, 2016, **152**, 504–512.
44 J. H. Zeng, J. Su and Z. H. Li, *Adv. Mater.*, 2005, **17**, 2119–2123.

45 H. X. Mai, Y. W. Zhang, R. Si, Z. G. Yan, L. D. Sun, L. P. You and C. H. Yan, *J. Am. Chem. Soc.*, 2006, **128**, 6426–6436.
46 (*a*) H. X. Mai, Y. W. Zhang, L. D. Sun and C. H. Yan, *J. Phys. Chem. C*, 2007, **111**, 13730–13739; (*b*) G. S. Yi, H. C. Lu, S. Y. Zhao, Y. Ge, W. J. Yang and D. P. Chen, *Nano Lett.*, 2004, **4**, 2191–2196.
47 Y. Wei, F. Q. Lu, X. R. Zhang and D. P. Chen, *J. Alloys Compd.*, 2007, **427**, 333–341.
48 H. J. Chang, J. Xie, B. Z. Zhao, B. T. Liu, S. L. Xu, N. Ren, X. J. Xie, L. Huang and W. Huang, *Nanomaterials*, 2014, **5**, 1–25.
49 G. S. Yi and G. M. Chow, *Adv. Funct. Mater.*, 2006, **16**, 2324–2329.
50 B. Zhou, L. Tao, Y. H. Tsang and W. Jin, *J. Mater. Chem. C*, 2013, **1**, 4313–4318.
51 H. Wang, Y. Liu and Z. Wang, *Nanoscale*, 2018, **30**, 10641–10649.
52 Y. Hu, B. Wu and Q. Jin, *Talanta*, 2016, **33**, 152–504.
53 Y. Y. Jin, D. L. Ni, L. Gao, X. F. Meng, Y. Lv, F. Han, H. Zhang, Y. Y. Liu, Z. W. Yao, X. Y. Feng, W. B. Bu and J. W. Zhang, *Adv. Funct. Mater.*, 2018, **28**, 1802656–1802663.
54 M. Šupová, *Ceram. Int.*, 2015, **41**, 9203–9231.